Homoepitaxial Branching: An Unusual Polymorph of Zinc Oxide Derived from Seeded Solution Growth

Rajeevan Kozhummal,[†,‡,§] Yang Yang,[†,*] Firat Güder,[†] Andreas Hartel,[†] Xiaoli Lu,[⊥] Umut M. Küçükbayrak,[†] Aurelio Mateo-Alonso,[‡,#,∥] Miko Elwenspoek,[‡,§] and Margit Zacharias[†,‡]

[†]Nanotechnology, Institute of Microsystems Engineering (IMTEK), Albert Ludwigs University of Freiburg, Georges-Köhler-Allee 103, D-79110 Freiburg, Germany, [‡]School of Soft Matter Research, Freiburg Institute for Advanced Studies (FRIAS), Albert Ludwigs University of Freiburg, Albertstraße 19, D-79104 Freiburg, Germany, [§]Transducers Science and Technology (TST), MESA+ Institute for Nanotechnology, University of Twente, PO Box 217, 7500 AE, Enschede, The Netherlands, [⊥]State Key Discipline Laboratory of Wide Band Gap Semiconductor Technology, School of Microelectronics, Xidian University, 710071 Xi'an, China, [#]POLYMAT, University of the Basque Country UPV/EHU, Avenida de Tolosa 72, E-20018 Donostia-San Sebastian, Spain, and [∥]Ikerbasque, Basque Foundation for Science, E-48011 Bilbao, Spain

ABSTRACT The development of hydrothermal synthesis has greatly promoted bottom-up nanoscience for the rational growth of diverse zinc oxide (ZnO) nanostructures. In comparison with normal ZnO nanowires, ZnO nanostructures with a larger surface area, for instance, branched nanowires, are more attractive in the application fields of catalysis, sensing, dye-sensitized solar cells *etc*. So far the ZnO branched nanowires achieved by either one-step or multistep growth always present a boundary-governed nonepitaxial branch/stem interface. In this report, seeded growth of single-crystalline ZnO hexabranched nanostructures was achieved by selecting polyethylene glycol (PEG) as capping agent based on a low-temperature, laterally epitaxial solution growth strategy. We investigated the generality of this PEG-assisted growth process using different ZnO seed layers including continuous film, patterned dots, and vertically aligned nanowire arrays. It was revealed that PEG is a distinctive *c*-direction inhibitor responsible for the lateral growth and subsequent branching of ZnO due to its nonionic and nonacidic feature and weak reactivity in the solution system. All the obtained branched nanostructures are of single crystallinity in nature, which is methodologically determined by the homoepitaxial growth mode. This PEG-assisted process is versatile for diameter tuning and branch formation of ZnO nanowires by secondary growth. Our proof-of-concept experiments demonstrated that the ZnO hexabranched nanostructures presented superior photocatalytic efficiency for dye degradation relative to the normal ZnO nanowires.

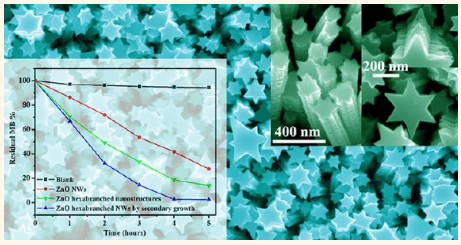

KEYWORDS: branching · epitaxial growth · structure-directing agent · ZnO nanowires · photocatalytic degradation

Zinc oxide (ZnO) is an important multifunctional semiconducting oxide that is widely used in energy conversion, electronics, optics, catalysis, and sensing.[1−12] The development of hydrothermal synthesis over the past decade has greatly promoted bottom-up nanoscience for the rational growth of diverse ZnO nanostructures.[6−17] The general merits of this strategy lie in low cost, low synthesis temperature, mild and environmentally benign reaction conditions, and easy scaling up. Moreover, a distinctive advantage emerging *via* this approach is the possibility of providing ZnO nanostructures with specific morphology or arrangement, which are directly linked to the functional requirements of practical devices for optimal performance.[6−12,18,19] For instance, well-aligned crystalline ZnO nanowires have been grown on flexible organic substrates, compatible with the design of inorganic−organic hybrid LEDs.[18] High-throughput fabrication of patterned ZnO nanowire arrays on a wafer scale has been readily achieved by combination with different lithography techniques, which is especially of use for ZnO-based light emitters and electrochromic displays.[19] By introducing capping agents with preferential binding abilities on specific ZnO crystal surfaces in low-temperature alkaline hydrothermal synthesis, systematic manipulation of the aspect ratio of ZnO nanowires has been accomplished toward the goal of morphology-coupled photocatalytic activity or field emission.[8,10]

Recently solution-grown ZnO nanowire arrays have been exploited in dye-sensitized solar cells (DSSCs) as an efficient photoanode alternative to traditional TiO_2 nanoparticle films.[3,6,9−11] However, the insufficient surface area of simple 1D ZnO nanostructures is unprofitable for high dye loading and light harvesting, which yet restricted the energy conversion efficiency to relatively low levels.[3] This weakness has been partly overcome by constructing DSSCs using ZnO nanowires with branched structures as photoanodes, which significantly improved the DSSC power conversion efficiency due

* Address correspondence to yang.yang@imtek.de.

Received for review May 17, 2012 and accepted July 31, 2012.

Published online July 31, 2012
10.1021/nn302188q

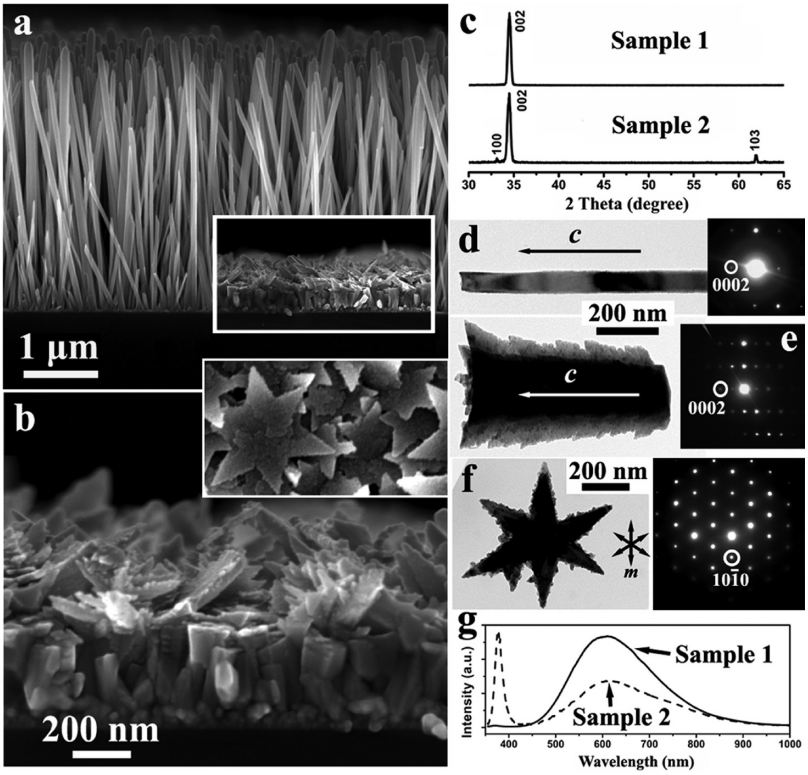

Figure 1. (a) Cross-sectional SEM image of as-grown ZnO nanowires (sample 1). Inset shows cross-sectional SEM image of ZnO branched nanorods (sample 2) with the same magnification. (b) Zoom-in of cross-sectional SEM image of sample 2 and its top view (inset). (c) XRD patterns of samples 1 and 2 for investigating the crystal structure and orientation. TEM images of individual nanostructures from sample 1 (d) and sample 2 (e, f) together with their SAED patterns. (g) PL spectra of samples 1 and 2 at room temperature.

to a greatly augmented ZnO surface area.[6,11] However, so far the branched ZnO nanowires achieved by either one-step or multistep growth always present a boundary-governed nonepitaxial branch/stem interface,[6,11,12,20−23] which is supposed to generate an additional bottleneck for DSSC efficiency due to the amplified charge recombination during boundary percolation. In view of the above facts, a single-crystalline ZnO branched nanostructure is practically imperative for photovoltaic applications owing to its high loading ability without sacrificing efficient electron transport. In this work, we demonstrate a versatile homoepitaxial solution synthesis strategy for seeded growth of single-crystalline ZnO hexabranched nanowires by selecting polyethylene glycol (PEG) as capping agent. This polymorph, which has been missing for a long time, may fill the void in the gallery of solution-grown ZnO nanostructures.

RESULTS AND DISCUSSION

To serve as the seed layer for the subsequent growth, atomic layer deposition (ALD) was used to grow a uniform ZnO film with a thickness of 30 nm on Si substrates. The as-deposited ZnO film presents no preferred orientation, which could be slightly improved by postannealing at elevated temperatures (Supporting Information, Figure S1). The substrate with the seed layer (1.5 cm^2) was placed facing downward into a 15 mL growth solution containing 12.5 mM zinc nitrate and 12.5 mM hexamethylenetetramine (HMTA) and then maintained at 90 °C for 24 h (sample 1).[17] Sample 2 was grown by the same procedure, but with the addition of 1 mL of PEG (M_w 400) in the starting solution.

Figure 1a shows a cross-sectional SEM image of sample 1 formed under the normal growth conditions, in which vertically aligned nanowire arrays about 80 nm in diameter and 3.5 μm in length are observed. The inset in Figure 1a illustrates the morphology of sample 2, where the height of the formed nanostructures was significantly reduced to only 500 nm in the presence of PEG in the growth solution. A close view shown in Figure 1b indicates the formation of a much denser film consisting of irregular rod-like nanostructures in sample 2. The top view (inset) reveals that each nanorod indeed has a uniform six-angle-star-like branched cross-section configuration.

XRD patterns in Figure 1c confirmed the formation of phase-pure hexagonal wurtzite ZnO nanostructures in both the samples. However, only sample 1 presents a highly [0001] preferred orientation. It is known that growth of ZnO along the [0001] direction (*c*-axis) is thermodynamically favored.[1] When ZnO nanowires started to grow from the non-highly oriented seeds,

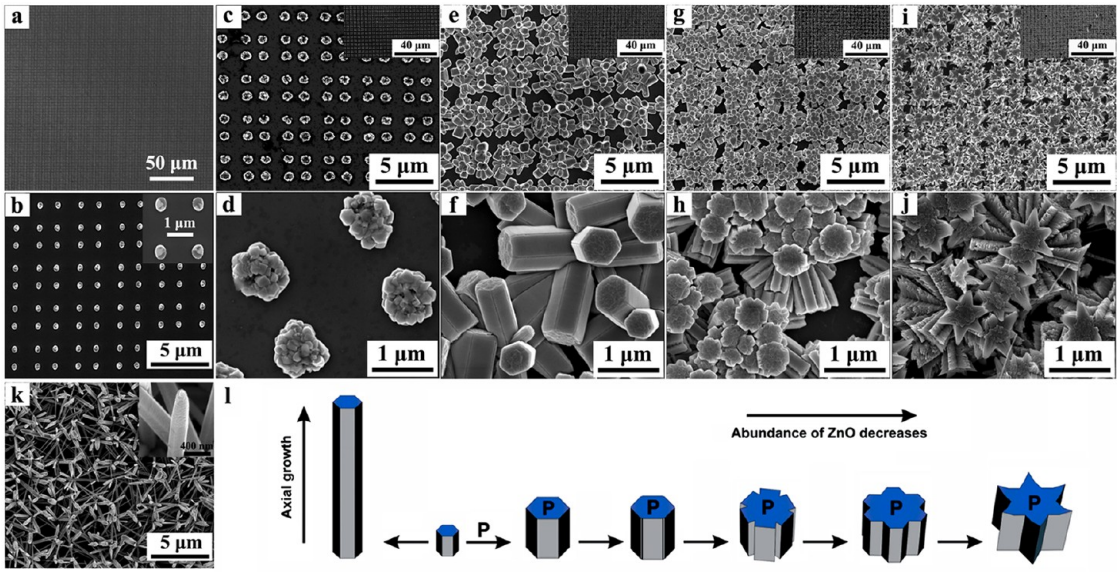

Figure 2. SEM images of patterned ZnO seed arrays by phase shift photolithography (a, b). Time-dependent morphological evolution of ZnO nanostructures grown from the seed arrays in the presence of 1 mL of PEG: 1 h (c, d); 9 h (e, f); 12 h (g, h); 24 h (i, j). Morphology of ZnO nanostructures grown from the seed arrays without PEG by 24 h (k). Each inset in (c), (e), (g), and (i) shows a corresponding general view. (l) Pictorial representation of the mechanism for the formation of single-crystalline ZnO hexabranched nanostructures. PEG is represented as P in the scheme.

a small amount of initial nanowires that were not aligned normal to the substrate was quickly impeded by neighboring crystals. Most vertical nanowires easily survived through competition and continued to grow, eventually forming [0001]-oriented arrays. As shown in Figure 1b, the very limited axial growth of sample 2 could not completely jump the traces of the underlying seed orientation. Thus, a relatively poor [0001] orientation was presented.

The TEM image in Figure 1d shows an individual ZnO nanowire of sample 1 and its related SAED pattern. The nanowire is single-crystalline and elongating along the inherent fast growth direction [0001] of ZnO. The nanorod of sample 2 in Figure 1e follows the same *c*-oriented growth habit. Although the nanorod has a rough surface with an unusual edge contrast under electron beam, it presents good single crystallinity. In addition, its diameter gradually declines from top to bottom. On condition that the nanorods are located on the (0001) basal plane, the configuration of six symmetric branches radiating from a stem was clearly verified (Figure 1f). The direction of extension of each branch corresponds to each *m*-orientation of six {10−10} axes symmetrically distributed in the ZnO (0001) foil plane. Figure 1g shows PL spectra of both the samples. The UV to visible emission ratio of sample 2 is much higher than sample 1, indicating a lower defect density in the ZnO hexabranched nanorods.[1]

PEG (M_w 400) is a common short-chain polymer with −(CH_2-CH_2-O)− repeating units. Previously, it was found that PEG could be exploited as a *c*-orientation crystal growth inhibitor only to selectively promote the formation of ZnO nanowires or nanorods in solution due to the coordination abilities of its oxygen atoms with zinc ions.[24] However, for the PEG-assisted ZnO growth based on the heterogeneous nucleation from the preformed seeds, the single-crystalline hexabranched polymorph was first discovered. We observed that even for the ZnO bipod crystals unavoidably precipitated in the bulk growth solution, the dominating evolution mode conformed to the fusion and stacking of neighboring ZnO blocks with a star-like morphology (Figure S2), different from all the reported cases in the literature.[20−22] Under the same reaction conditions, fractal and tapered nanotrees were formed when the concentrations of zinc nitrate and HMTA in the nutrient solution were synchronously halved while the PEG amount was maintained (Figure S2). Inversely, drastic increase of the PEG amount while the reactant concentrations remained unchanged induced the formation of thinner and flatter ZnO evolving from nanoplates to nanoslices (Figure S2). The above findings strongly hinted that PEG is probably a previously "underestimated" structure-directing agent, which is practically *versatile* for the geometric regulation of the solution-grown ZnO nanostructures. Therefore, the specific role of PEG in the seeded growth of ZnO will be revisited.

For a better understanding of how the single-crystalline ZnO hexabranched nanorods developed under the assistance of PEG, we conducted a time-dependent synthetic study. In order to maximally weaken the influence of steric hindrance on the structure evolution (discerned in Figure 2b), patterned ZnO dots were used as the seeds instead of the continuous ZnO film. From a technical point of view, it is still challenging to

manipulate the building blocks of functional nanostructures into a large-scale regular form, which is essential for future advanced integration-compatible devices.[19,25] Patterned ZnO dots were generated by a modified phase shift photolithography technique.[25] In brief, a 30 nm ALD ZnO layer deposited on a Si wafer was first coated with a positive resist. The patterned resist dot masters were formed by double-exposure near-field phase shift lithography and were further used as an etch mask to create patterned ZnO seed arrays (Figure S3). As shown in Figure 2a, b, square patterns of ZnO dots with diameters of <400 nm were readily created with perfect periodic order on a large scale.

Figure 2c–j shows the PEG-assisted evolution of ZnO from the patterned dot arrays at selected time intervals, *viz*., 1, 9, 12, and 24 h. In all the stages, the emergence of diverse nanostructures was exclusively centered at each dot, persisting with the initial periodicity (also see Figure S4). After the reaction for 1 h (Figure 2c, d), multiple nucleation sites arose from each polycrystalline dot. Up to 9 h (Figure 2e, f), the growth occurred both axially and laterally, leaving thick hexagonally prismatic structures. In all these structures axial stripes can be detected along all six prism edges. A longer reaction time of 12 h resulted in negligible growth along both directions (Figure 2g, h). The immediate structures have an apparent 18-sided shape with a flat top surface. The stripes observed in the previous phase have been changed to deeper axial grooves that separate six outspread branches. At a latter reaction stage from 12 to 24 h, the branches elongated, sharpened, and slightly turned up at the tips, leading to the formation of hexabranched nanostructures with a six-angle-star-like cross-section, as shown in Figure 2i, j. Note that the diameter of most ZnO nanostructures formed in the latter stages shrank from the top toward the nucleation sites (Figure 2h, j). Figures 2k shows the morphology of ZnO grown from the patterned dot arrays after a 24 h reaction without PEG. As expected, slim nanowires with a tapered end were obtained. The unrestricted extension of nanowires from differently oriented nuclei almost obscured the patterned structure (Figure S5).

On the basis of the above observations, we propose a possible growth mode for the ZnO hexabranched nanostructures. A graphical illustration is also presented in Figure 2l. At the initial stage, tiny ZnO nuclei with faceted surfaces were grown from the seeds by competitive nucleation. The Zn^{2+}-terminated (0001) surface was specifically capped by PEG *via* coordination with oxygen atoms, which suppressed the growth of ZnO on this thermodynamically preferred surface. Initially, the precursor in the solution was abundant and the growth occurred axially (*c*-axis) in a low rate together with the enhanced lateral growth. Thick hexagonal prismatic structures were thus produced.

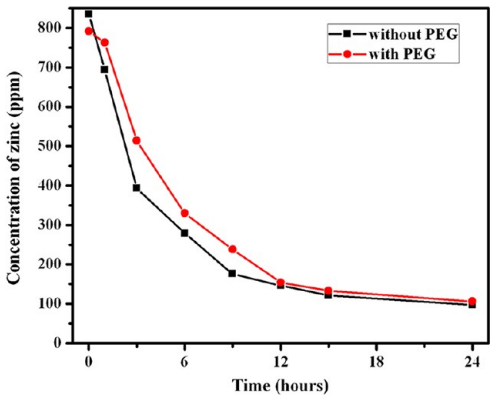

Figure 3. Relation between the overall Zn concentration in the growth solution and the reaction time with and without PEG. Prior to the AAS measurement, each growth solution was centrifuged at 4000 rpm for 10 min to remove possible precipitates.

With the gradual depletion of Zn^{2+} ions in a prolonged reaction process, the growth of ZnO slowed and got close to the growth–dissolution equilibrium.[26] Because the fast etching (0001)-plane of ZnO was efficiently capped by PEG, the six prismatic edges intersecting adjacent *m*-planes became the most unstable fronts. The dissolution of ZnO on the edges was faster than its reprecipitation, which initiated six axial etched stripes and gradually deepened them. In contrast, the prism faces at the growth fronts continued to extend and branched epitaxially along the six *m*-axes. As the reaction further proceeded, the increasingly limited supply of the reactant precursor ended the branches with tips.[27]

To confirm the branching mechanism we proposed above, we further measured the actual concentration of overall soluble Zn species (simplified as Zn ions) in the growth solution with PEG during different reaction stages by atomic absorption spectrometer (AAS). Here, continuous ZnO films were used as the seed layer. All the other reaction parameters followed the standard setup in our experiments. By analyzing the AAS result (red plot) shown in Figure 3, it can be seen that the concentration of Zn ions in the growth solution decreased significantly from 800 to 340 ppm during the initial 6 h for the ZnO-forming reaction. In this stage, heterogeneous nucleation of ZnO on the seeded substrate was favorable because the existing seeds bypassed the nucleation step.[17] On condition that the supersaturation of ZnO clusters was maintained in the solution, ZnO nanorods could form and continue to develop by anisotropic growth, although the growth along the *c*-orientation was severely restricted due to the presence of PEG. Within the next 6 h, the depletion of Zn ions started to slow. Accordingly, the growth rate of ZnO nanorods also decreased. Afterward, the concentration of Zn ions was only decreased from 150 ppm to 110 ppm up to 12 h before the end of the reaction. Therefore, only a slight depletion of Zn ions

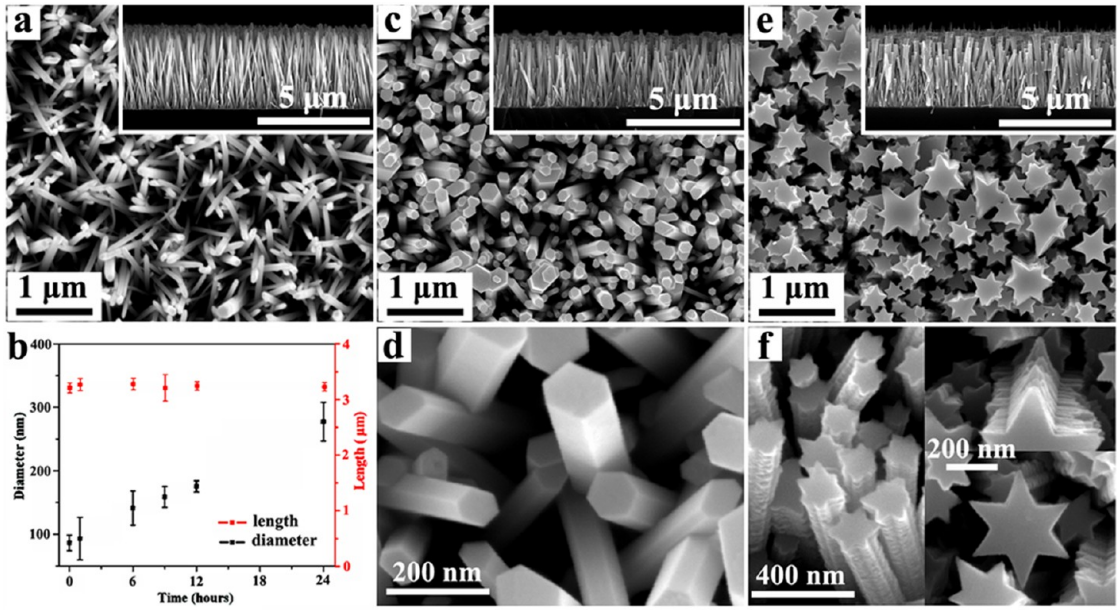

Figure 4. (a) SEM image of ZnO nanowires used as the seeds. (b) Plots of the average length (red) and diameter (black) of ZnO nanowires as a function of the growth time by the PEG-assisted secondary growth (1 mL of PEG). Morphologies of two important stages: 6 h (c, d) and 24 h (e, f). Inset in (a), (c), and (e) is a corresponding cross-sectional SEM image of each sample.

occurred during the latter 12 h, which confirmed that the system herein was in a state close to a dynamic equilibrium while the branching of ZnO nanowires occurred during this time window. The above AAS results provided crucial support for the proposed dissolution−reprecipitation mechanism that is responsible for the formation of ZnO hexabranched nanostructures. In addition, we also investigated the time-dependent change of the Zn concentration for the seeded solution growth without PEG. As presented in Figure 3 (black plot), the trend of the Zn concentration over time was similar to the system with PEG. Therefore, the depletion of Zn ions subjected to the ZnO-forming reaction was hardly influenced by the addition of PEG (1 mL) in the system. This result presented additional evidence for the nonacidic nature and weak reactivity of PEG in this solution reaction system.

Regarding the *c*-axis inhibitors, anionic citrate has been most popularly used to tune the aspect ratio of ZnO nanostructures.[14,20−22] Recently various metal complex ions also demonstrated efficient control of the morphology of ZnO nanostructures by face-selective electrostatic adsorption.[10] However, neither of the strategies has been found applicable for the branched nanostructure formation. We consider that the distribution of species responsible for the capping in the ionic inhibitors is extremely sensitive to the solution environment. Especially, the significantly decreased pH value accompanied by the limited precursor supply could convert the capping agents to invalid forms. For this reason, the layered ZnO nanostructures in the citrate-assisted process were still tapered along the *c*-axis, enduring a longer reaction time.[14,28] When more citrate ions were added, a porous structure with no alignment was formed due to the dissolution of ZnO,[28] most probably induced by the strong hydrolysis of concentrated citrate ions near the end of the reaction. Therefore, the formation of the branched nanostructures is greatly beneficial from the nonionic, nonprotic, and weak-reactive features of PEG, which represents a more effective structure-directing agent for ZnO solution growth.

Furthermore, we investigated the PEG-assisted approach for secondary growth using solution-grown ZnO nanowires as the seeds (Figure 4a). During the PEG-assisted secondary growth, the length and diameter of the evolving nanowires were investigated at different time intervals within 24 h (Figure S6). The relations of the average length and diameter as a function of the growth time are plotted in Figure 4b. It is clear that the nanowires hardly grew along [0001] direction with the *c*-axis inhibitor PEG, while lateral growth was favored, continuing throughout the secondary growth. In contrast, when the secondary growth was conducted in the nutrient solution without PEG, the initial ZnO nanowires slightly grew along the *c*-direction while the diameters remained unchanged (Figure S7).

For the PEG-assisted secondary growth, there are two important stages worth special mention. Compared with the seed nanowires, the ZnO nanowires by secondary growth up to 6 h are much thicker and more hexagonally faceted (Figure 4c, d). The unidirectional lateral growth mode governed by PEG indeed provides a potential solution route for achieving purposely doped homoepitaxial ZnO coaxial nanowires with selective incorporation of dopants into the regenerative shell. After 24 h of incubation, single-crystalline

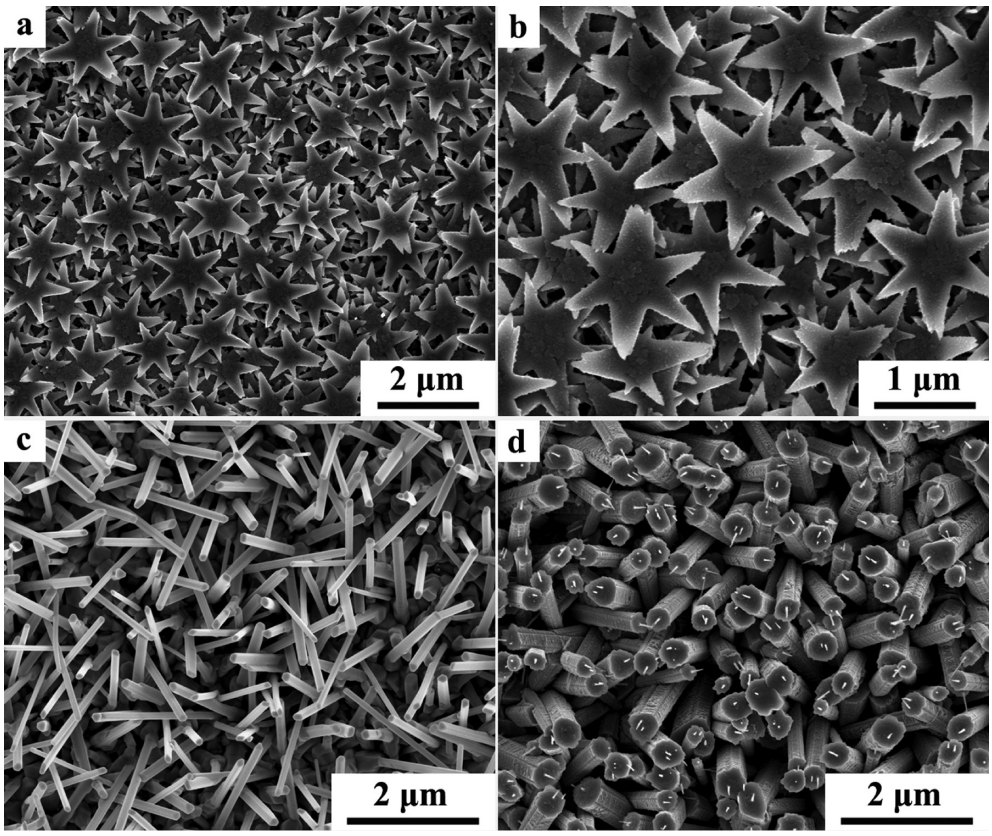

Figure 5. (a, b) SEM images of ZnO hexabranched nanowires after secondary growth using a piece of nanowire seed with a smaller size. (c) SEM image of long ZnO nanowires grown by chemical vapor deposition. (d) SEM images of ZnO hexabranched nanowires after secondary growth using the sample in (c) as the seeds. A very short and undeveloped branched configuration is shown. For both cases, the reaction was conducted at 90 °C for 24 h using 1 mL of PEG and 12.5 mM precursor concentrations for both $Zn(NO_3)_2$ and HMTA.

hexabranched nanowires with a six-angle-star-like cross-section were obtained (Figure 4e, f). Each nanowire is multilayered with a flat top surface and a uniform width from top to bottom. The free space between adjacent nucleation units in vertical nanowire seeds is much larger than those in the polycrystalline film and the patterned dots each consisting of multiple nuclei. Therefore, we consider that the upturned star tips and the reverse pyramidal shape occurring in the former cases (Figures 1b and 2j) were caused by gradually restricted diffusion of the aqueous precursor toward the bottoms of nuclei rather than the growth habit.

By tuning the PEG amount or precursor concentrations or both, diverse hierarchical 1D ZnO nanostructures were obtained by the secondary growth (Figures S8). Generally, increasing the PEG portion for fixed precursor concentrations more efficiently inhibited the *c*-direction growth and benefited the branching. When the PEG amount was insufficient, long helical ZnO nanowires were finally grown along the *c*-direction on the top of aligned ZnO hexabranched nanowires (Figure S9). When an excess PEG amount was added, the high viscosity of the nutrient solution severely retards the aqueous diffusion of precursors deep in the nanowire seeds, which again led to a reverse pyramidal geometry of the epitaxial structures (Figure S9). Therefore, 1−2 mL of PEG was suggested as an optimal window for the formation of uniform hexabranched nanowires in the current experimental setup. In addition, the intersection angle and the extent of six branches could also be adjusted by varying the number, diameter, or length of ZnO nanowires used as the seeds. Figure 5a, b shows SEM images of the ZnO hexabranched nanowires formed by secondary growth from a smaller piece of substrate containing solution-grown ZnO nanowire seeds with the same density. In contrast to the result presented in Figure 4e, longer branches accompanied with reduced intersection angles between adjacent branches can be clearly observed. The decrease in the number of ZnO nanowire seeds indeed increased the loading of ZnO precipitates averaged by each *m*-plane near the end of the reaction, so the branching could occur in a slower tapered fashion, leading to a more adequate development of the branches. Inversely, if the number of the same nanowire seeds is raised or the average diameter or length of each nanowire serving as the seed is significantly increased, a short and undeveloped branched configuration can be expected due to the

fast depletion of the limited ZnO precursors shared by excess *m*-plane areas. Figure 5c shows an SEM image of the ZnO nanowires grown by the chemical vapor deposition (CVD) method. Compared with the solution-grown ZnO nanowires shown in Figure 4a, these nanowires are much thicker and longer. When these CVD-grown ZnO nanowires were used as the seeds for the secondary growth subject to 24 h in the presence of PEG, ZnO nanowires with increased diameters and immature branched configuration were finally produced (Figure 5d), consistent with our postulation. This result also demonstrated that this PEG-assisted secondary growth process is compatible with primary ZnO nanowires produced by both solution and gas routes for achieving effective structural tuning.

ZnO has been known as a photocatalyst, displaying impressive applications in the photodegradation of some organic compounds.[8] To compare the photocatalytic activity of normal ZnO nanowires and ZnO branched nanostructures, we conducted photocatalyzed dye degradation experiments with the organic dye methylene blue (MB) under ultraviolet light. An aqueous solution of MB (4 mL, 2 μM) was separately prepared in 10 mL glass beakers. One sample solution was used as reference to measure the degradation without catalyst (blank). Two dye solutions were separately added with a piece of normal ZnO nanowire catalyst (2 cm^2) and a piece of hexabranched nanorod catalyst (2 cm^2), both of which were grown from continuous ZnO film seeds. The above solutions were kept overnight in the dark to establish an adsorption−desorption equilibrium. Then all three MB solutions were exposed to a UV lamp with a wavelength of 254 nm and a power of 15 W. At each time interval the irradiation was paused and solution from each sample was added to quartz cuvettes for absorbance measurement using a UV−vis spectrophotometer. After the measurement the solutions were returned to the beaker and the irradiation was resumed. As shown in Figure 6, after exposure to UV light for 4.0 h, the ZnO branched nanorods were able to degrade 82% of MB (green plot), whereas the normal ZnO nanowires degraded only 56% (red plot). The corresponding AAS results for these two samples (Figure 3) have evidenced that the concentration changes of Zn ions in the growth solution with and without PEG followed a similar trend and rate, indicating the products of both samples are comparable in amount. Moreover, when the morphologies of the nanowires and the branched nanorod samples are compared (Figure 1a), the branched nanorod sample showed a "negative" effect of the total ZnO volume (less volume) regarding its much lower height if the volume difference still existed. Therefore, the contribution from a larger volume of the hexabranched nanorod sample to the enhanced MB degradation efficiency was excluded. Because ZnO hexabranched nanorods with a large total surface area were enclosed by a greater proportion of (0001) polar faces with intrinsically the highest energy, the higher photocatalytic activity could be attributable to the larger polar surface area or larger total surface area or their synergetic effect.

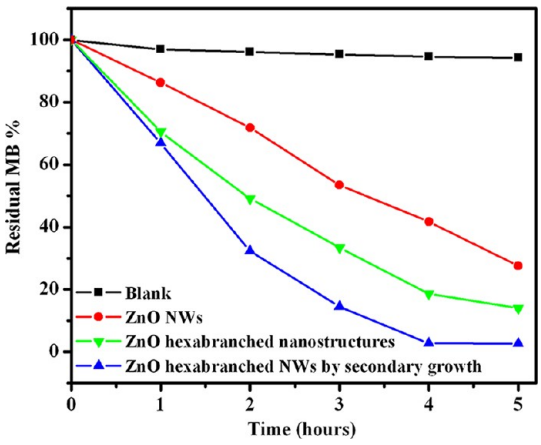

Figure 6. Degradation of MB photocatalyzed by normal ZnO nanowires (red), primary ZnO hexabranched nanorods (green), and secondarily grown ZnO hexabranched nanowires (blue) under UV irradiation.

Furthermore, we compared the photocatalytic activity of the ZnO hexabranched nanorods with the ZnO hexabranched nanowires *via* secondary growth of the normal nanowires. As shown in Figure 6 (blue plot), the ZnO branched nanowires formed by secondary growth degraded almost all the MB within 4.0 h, showing higher degradation efficiency. In contrast to the ZnO branched nanorods, the sample of ZnO branched nanowires formed by secondary growth has a nearly equal (0001) polar surface area, but significantly enlarged total volume and total surface area. However, the enhancement of its dye degradation efficiency fell far behind considering these augmentations. Therefore, it is reasonable to suggest that the proportion of polar surfaces in the ZnO hexabranched nanostructures plays a major role in the enhancement of the degradation of organic pollutants.[8]

CONCLUSIONS

In summary, the polymer PEG was introduced as a versatile structure-directing agent for aqueous seeded growth of single-crystalline ZnO hexabranched nanowires. We investigated the generality of this PEG-assisted growth process using different ZnO seed layers including continuous film, patterned dots, and vertically aligned nanowire arrays. All the obtained branched nanostructures are of single crystallinity in nature, which is methodologically determined by the homoepitaxial growth mode. Single-crystalline hexabranched nanowires are expected to find important applications in various fields such as UV photocatalysts for organic pollutant degradation and photoanodes for

DSSCs. Moreover, PEG reflects some properties of natural mucous membrane surfaces. The formation of such highly symmetrical complex structures induced by PEG in a mild environment might broaden our understanding of the mineralization of biomaterials.

EXPERIMENTAL SECTION

Materials. Zinc nitrate hexahydrate ($Zn(NO_3)_2 \cdot 6H_2O$), hexamethylenetetramine ($C_6H_{12}N_4$), polyethylene glycol (M_w 400), and methylene blue ($C_{16}H_{18}N_3SCl$) were procured from Sigma Aldrich and used without further purification.

Preparation of ZnO Seed Layers by Atomic Layer Deposition. A ZnO thin film was grown at 115 °C by reacting diethylzinc with water vapor in a vertical flow-type reactor (OpAL, Oxford Instruments) at pressures between 80 and 180 mTorr. Nitrogen gas was used as the carrier gas with a flow rate of 25 sccm.

Fabrication of Patterned ZnO Dot Arrays. A p-type Si(100) wafer was first coated with a 30 nm ALD ZnO layer. The ZnO layer was additionally coated with a positive tone photoresist (AZ 5214), which was patterned by double-exposure near-field phase shift lithography and developed in MIF 726 solution for approximately 1 min. Note that the used mask is an inexpensive homemade borosilicate mask. The obtained resist patterns were then used as an etch mask to create patterned ZnO seed arrays with diameters of <400 nm using reactive ion etching with a gas mixture of 16:34:5 sccm CHF_3/CF_4/Ar at 200 W of platen power. The etch duration was 4 min. Finally, the remaining photoresist residue was removed by acetone.

Synthesis of ZnO Nanowires and Hexabranched Nanostructures. Nanowires were prepared by the classic method. A 15 mL amount of a 12.5 mM solution of zinc nitrate and HMTA was contained in a glass tube. A piece of silicon (3 cm × 0.5 cm) with a continuous annealed ZnO ALD layer or patterned ZnO dot array was inserted into the solution slantwise. The bottle was sealed and kept at 90 °C for 24 h. After 24 h the solution was cooled and the sample was washed with deionized (DI) water and dried naturally. For hexabranched nanostructures, in addition to the precursor solution, 1 mL of PEG was added to the solution and the experiment was conducted in the same way.

Secondary Growth of ZnO Hexabranched Nanowires. In a typical experiment, nanowire samples of dimensions 3 cm × 0.5 cm prepared as described above were placed in 15 mL of precursor solution (zinc nitrate and HMTA, 12.5 mM) added with 1 mL of PEG. The bottle was sealed and kept at 90 °C for 24 h. After 24 h the solution was cooled and the sample was washed with DI water and dried naturally.

Preparation of ZnO Nanowires by Chemical Vapor Deposition. Nanowires were grown on Si substrate with Au as catalyst in a two-zone furnace. The substrate was prepared by evaporating a film of Au on a piece of silicon wafer. The substrate was placed inside the quartz tube at the downstream position in the first heating zone of the furnace. A 1 g sample of the source containing ZnO powder (99.999%) and powdered graphite (99.99%) in 1:1 ratio was placed in the second heating zone of the furnace. The tube was evacuated to a pressure of 4×10^{-5} mbar. Then O_2 and Ar were set to flow through the tube at flow rates of 1.5 and 30 sccm, respectively. The first heating zone was kept at 750 °C and the second zone at 950 °C. The heating was continued for 1 h and then cooled, the vacuum was released, and the sample was taken out of the furnace.

Characterization. High-resolution SEM images were obtained using a Nova NanoSEM (FEI) SEM. TEM images of the ZnO nanostructures and the corresponding ED pattern were obtained by using a JEOL 1010 microscope at an accelerating voltage of 100 kV. The nanostructures were scratched from the Si substrate, dispersed in ethanol (analytically pure, 99.99%), dip-coated onto a copper grid coated with a thin carbon film, and dried at room temperature. The crystal structure was characterized by XRD $\theta-2\theta$ scans using a Philips X'Pert MRD diffractometer with Cu Kα radiation. Photoluminescence (PL) measurements were carried out using the 514.5 nm line of an Ar^+ ion laser with an excitation power of 14 mW. PL spectra were measured at room temperature with a LN_2-cooled CCD camera attached to a single grating monochromator using a HeCd laser (3.8 eV line) as excitation source. All the spectra were corrected for the spectral response of the setup. The concentration of Zn ions in the growth solution at different reaction stages was determined by an Analytik Jena Vario 6 atomic absorption spectrometer. The samples were centrifuged at 4000 rpm for 10 min to remove any precipitates before the measurements.

Photocatalytic Activity. The photocatalytic activities of various ZnO nanostructures grown on a Si substrate were investigated by using organic dye degradation under ultraviolet light. The test solution was an aqueous solution of methylene blue (4 mL, 2 μM) stored in a 10 mL glass beaker. The initial absorbance was measured by using a UV−vis spectrophotometer (Perkin-Elmer, Lambda 950). Then all the solutions with and without ZnO photocatalysts were exposed to UV (UV lamp XX-15S (UVP Inc.)) with a wavelength of 254 nm and a power of 15 W. At each time interval the irradiation was paused and solution from each sample was moved to a quartz cuvette for absorbance measurement. After the measurement the solutions were returned to the beaker and the irradiation was resumed.

Conflict of Interest: The authors declare no competing financial interest.

Acknowledgment. Financial support from German Research Foundation (DFG) under contract ZA 191/24-1 and Freiburg Institute for Advanced Studies (FRIAS) is gratefully acknowledged.

Supporting Information Available: Control experiments. This material is available free of charge *via* the Internet at http://pubs.acs.org.

REFERENCES AND NOTES

1. Morkoç, H.; Özgür, U. *Zinc Oxide: Fundamentals, Materials and Device Technology*; Wiley-VCH: Weinheim, 2009.
2. Huang, M. H.; Mao, S.; Feick, H.; Yan, H. Q.; Wu, Y. Y.; Kind, H.; Weber, E.; Russo, R.; Yang, P. D. Room-Temperature Ultraviolet Nanowire Nanolasers. *Science* **2001**, *292*, 1897–1899.
3. Law, M.; Greene, L. E.; Johnson, J. C.; Saykally, R.; Yang, P. D. Nanowire Dye-Sensitized Solar Cells. *Nat. Mater.* **2005**, *4*, 455–459.
4. Patolsky, F.; Lieber, C. M. Nanowire Nanosensors. *Mater. Today* **2005**, *8*, 20–28.
5. Wang, Z. L.; Song, J. H. Piezoelectric Nanogenerators Based on Zinc Oxide Nanowire Arrays. *Science* **2006**, *312*, 242–246.
6. Jiang, C. Y.; Sun, X. W.; Lo, G. Q.; Kwong, D. L.; Wang, J. X. Improved Dye-Sensitized Solar Cells with a ZnO-Nanoflower Photoanode. *Appl. Phys. Lett.* **2007**, *90*, 263501(3pp).
7. Liang, W.; Yuhas, B.; Yang, P. Magnetotransport in Co Doped ZnO Nanowires. *Nano Lett.* **2009**, *9*, 892–896.
8. Mclaren, A.; Valdes-Solis, T.; Li, G.; Tsang, S. C. Shape and Size Effects of ZnO Nanocrystals on Photocatalytic Activity. *J. Am. Chem. Soc.* **2009**, *131*, 12540–12541.
9. Briseno, A. L.; Holcombe, T. W.; Boukai, A. I.; Garnett, E. C.; Shelton, S. W.; Fréchet, J. M. J.; Yang, P. Oligo- and Polythiophene/ZnO Hybrid Nanowire Solar Cells. *Nano Lett.* **2010**, *10*, 334–340.
10. Joo, J.; Chow, B. Y.; Prakash, M.; Boyden, E. S.; Jacobson, J. M. Face-Selective Electrostatic Control of Hydrothermal Zinc Oxide Nanowire Synthesis. *Nat. Mater.* **2011**, *10*, 596–601.
11. Ko, S. H.; Lee, D.; Kang, H. W.; Nam, K. H.; Yeo, J. Y.; Hong, S. J.; Grigoropoulos, C. P.; Sung, H. J. Nanoforest of Hydrothermally Grown Hierarchical ZnO Nanowires for a High

Efficiency Dye-Sensitized Solar Cell. *Nano Lett.* **2011**, *11*, 666–671.
12. Qiu, Y.; Yan, K.; Deng, H.; Yang, S. Secondary Branching and Nitrogen Doping of ZnO Nanotetrapods: Building a Highly Active Network for Photoelectrochemical Water Splitting. *Nano Lett.* **2012**, *12*, 407–413.
13. Taubert, A.; Palms, D.; Weiss, O.; Piccini, M.; Batchelder, D. N. Polymer-Assisted Control of Particle Morphology and Particle Size of Zinc Oxide Precipitated from Aqueous Solution. *Chem. Mater.* **2002**, *14*, 2594–2601.
14. Tian, Z. R.; Voigt, J. A.; Liu, J.; Mckenzie, B.; Mcdermott, M. J.; Rodriguez, M. A.; Konsishi, H.; Xu, H. Complex and Oriented ZnO Nanostructures. *Nat. Mater.* **2003**, *2*, 821–826.
15. Greene, L.; Law, M.; Tan, D. H.; Goldberger, J.; Yang, P. General Route to Vertical ZnO Nanowire Arrays Using Textured ZnO Seeds. *Nano Lett.* **2005**, *5*, 1231–1236.
16. Xu, S.; Wei, Y.; Kirkham, M.; Liu, J.; Mai, W.; Davidovic, D; Snyder, R. L.; Wang, Z. L. Patterned Growth of Vertically Aligned ZnO Nanowire Arrays on Inorganic Substrates at Low Temperature without Catalyst. *J. Am. Chem. Soc.* **2008**, *130*, 14958–14959.
17. Xu, S.; Wang, Z. L. One-Dimensional ZnO Nanostructures: Solution Growth and Functional Properties. *Nano Res.* **2011**, *4*, 1013–1098.
18. Xu, S.; Shen, Y.; Ding, Y.; Wang, Z. L. Growth and Transfer of Monolithic Horizontal ZnO Nanowire Superstructures onto Flexible Substrates. *Adv. Funct. Mater.* **2010**, *20*, 1493–1497.
19. Wei, Y.; Wu, W.; Guo, R.; Yuan, D.; Das, S.; Wang, Z. L. Wafer-Scale High-Throughput Ordered Growth of Vertically Aligned ZnO Nanowire Arrays. *Nano Lett.* **2010**, *10*, 3414–3419.
20. Zhang, T.; Dong, W.; Keeter-Brewer, M.; Konar, S.; Njabon, R. N.; Tian, Z. R. Site-Specific Nucleation and Growth Kinetics in Hierarchical Nanosyntheses of Branched ZnO Crystallites. *J. Am. Chem. Soc.* **2006**, *128*, 10960–10968.
21. Sounart, T. L.; Liu, J.; Voigt, J. A.; Hsu, J. W. P.; Spoerke, E. D.; Tian, Z.; Jiang, Y. Sequential Nucleation and Growth of Complex Nanostructured Films. *Adv. Funct. Mater.* **2006**, *16*, 335–344.
22. Sounart, T. L.; Liu, J.; Voigt, J. A.; Huo, M.; Spoerke, E. D.; McKenzie, B. Secondary Nucleation and Growth of ZnO. *J. Am. Chem. Soc.* **2007**, *129*, 15786–15793.
23. Zhao, F.; Zheng, J.; Yang, X.; Li, X.; Wang, J.; Zhao, F.; Wong, K. S.; Liang, C.; Wu, M. Complex ZnO Nanotree Arrays with Tunable Top, Stem and Branch Structures. *Nanoscale* **2010**, *2*, 1674–1683.
24. Li, Z.; Xiong, Y.; Xie, Y. Selected-Control Synthesis of ZnO Nanowires and Nanorods *via* a PEG-Assisted Route. *Inorg. Chem.* **2003**, *42*, 8105–8109.
25. Henzie, J.; Barton, J. E.; Stender, C. L.; Odom, T. W. Large-Area Nanoscale Patterning: Chemistry Meets Fabrication. *Acc. Chem. Res.* **2006**, *39*, 249–257.
26. Yin, S.; Sato, T. Mild Solution Synthesis of Zinc Oxide Films with Superhydrophobicity and Superhydrophilicity. *J. Mater. Chem.* **2005**, *15*, 4584–4587.
27. Lv, Y.; Li, C.; Guo, L.; Wang, Q.; Wang, R.; Xu, H.; Yang, S.; Ai, X.; Zhang, J. Nanostructured Stars of ZnO Microcrystals with Intense Stimulated Emission. *Appl. Phys. Lett.* **2005**, *87*, 163103.
28. Bendall, J. S.; Visimberga, G.; Szachowicz, M.; Plank, N. O. V.; Romanov, S.; Sotomayor-Torres, C. M.; Welland, M. E. An Investigation into the Growth Conditions and Defect States of Laminar ZnO Nanostructures. *J. Mater. Chem.* **2008**, *18*, 5259–5266.